Applied Physics Express

The Japan Society of Applied Physics

LETTERS

# Revealing microstructure and dislocation behavior in BAlN/AlGaN heterostructures

To cite this article: Haiding Sun *et al* 2018 *Appl. Phys. Express* **11** 011001

# Microstructure revealing and dislocation behavior in BAlN/AlGaN heterostructures

Haiding Sun[1], Feng Wu[1], Young Jae Park[2], T. M. Al tahtamouni[3], Che-Hao Liao[1], Wenzhe Guo[1], Nasir Alfaraj[1], Kuang-Hui Li[1], Dalaver H. Anjum[4], Theeradetch Detchprohm[2], Russell D. Dupuis[2], Xiaohang Li[1]

[1] King Abdullah University of Science and Technology (KAUST), Advanced Semiconductor Laboratory, Thuwal, 23955-6900, Saudi Arabia

[2] Center for Compound Semiconductors and School of Electrical and Computer Engineering, Georgia Institute of Technology, Atlanta, Georgia 30332, USA

[3] Materials Science and Technology Program, College of Arts and Sciences, Qatar University, Doha 2713, Qatar

[4] King Abdullah University of Science and Technology (KAUST), Imaging and Characterization Core Laboratory, Thuwal 23955-6900, Saudi Arabia

We reveal the microstructure and dislocation behavior in a 20-pair $B_{0.14}Al_{0.86}N/Al_{0.70}Ga_{0.30}N$ multiple-stack heterostructures (MSHs) which exhibited an increasing dislocation density along the *c*-axis that is attributed to the continuous generation of dislocations (edge and mixed-type) within individual $B_{0.14}Al_{0.86}N$ layers. At the MSH interfaces, the threading dislocations were accompanied by a string of V-shape pits extending to the surface, leading to interface roughening and the formation of surface columnar features. Strain maps indicated an approximately 1.5% tensile and 1% compressive strain in the $B_{0.14}Al_{0.86}N$ and $Al_{0.70}Ga_{0.30}N$ layers respectively. Twin structures were observed and the MSH eventually turned from monocrystalline to polycrystalline.

Boron-Aluminum-Nitride (BAlN) is an emerging III-nitride alloy and possesses large bandgap comparable to that of AlN and Al-rich AlGaN.[1] In particular, it is promising for DUV distributed Bragg reflectors (DBRs) and thus surface-emitting lasers. [2] This is due to the considerable reduction of refractive index with the increase of boron (B) content with respect to AlN.[3] Moreover, our recent study of band alignment of the BAlN/AlGaN heterojunction shows its potentials for the electron-blocking layers of optoelectronics and barriers of power electronics devices due to the unique band offset with conventional InAlGaN alloys.[4] Despite the potential of BAlN, the scope of experimental studies has been rather limited, especially in relation to the growth of single-phase wurtzite BAlN layers with relatively high B content and large thickness. Earlier reports on BAlN alloy growth showed merely 1-2% B content in the layers due to phase separation, limited B diffusion, and parasitic reactions.[5] Li *et al*., demonstrated a much higher B content of 12%.[6,7] However, the single-phase wurtzite structure was only observed in the first 10 nm or a thinner region of the BAlN layers. Above that, a polycrystalline phase was formed which is undesirable in a wurtzite device structures. Recently, we demonstrated a significant increase of thickness (i.e., 100 nm) and B content up to 14.4% for single-phase wurtzite BAlN layers. [8,9] The result provides the foundation for the development of BAlN-based heterostructures.

For the BAlN/AlN heterostructures, Abid and Li *et al*., have performed growth and characterization studies.[3,7] However, these studies were constrained by the small thickness of the wurtzite phase. Besides, it is worth pointing out that the application of the BAlN/AlN heterostructures could be limited because of the similar properties such as the bandgap, band offset, and refractive index even for the non-active device layer. In addition, we have found that the bandgap of BAlN transitions from direct to indirect bandgap as B content increased to 12%.[1] This result indicates that it is unlikely for BAlN to be the sole material for the active layer of future high-performance DUV devices. Therefore, BAlN would probably have to be integrated with Al-rich AlGaN to form heterostructures for the applications in the DUV devices. So far,

there have been limited experimental reports concerning the structural characterization of BAlN/AlGaN heterostructures with high B content.

In this study, we performed the growth of BAlN/AlGaN multiple stack heterostructures (MSHs) using metalorganic chemical vapor deposition (MOCVD). We conducted detailed characterizations related to the microstructure, defect formation and strain within the BAlN and AlGaN layers. Our experimental analysis would provide insights for future research and development of the BAlN/AlGaN heterostructures by improving the quality of such junctions.

The MSHs of this study comprised 20 pairs of 35 nm $B_{0.14}Al_{0.86}N$/30 nm $Al_{0.7}Ga_{0.3}N$, and were grown on a 3 µm thick AlN template layer on a *c*-plane sapphire substrate,[10, 11] with the first and last MSH layers being $B_{0.14}Al_{0.86}N$ and $Al_{0.7}Ga_{0.3}N$, respectively. The AlN templates have a roughness of ~0.5 nm with an estimated threading dislocation density of ~ $10^9/cm^2$. The details of the AlN templates can be found in Ref 10 and 11. The MSH layer thicknesses were chosen to match the ones of a $B_{0.14}Al_{0.86}N/Al_{0.7}Ga_{0.3}N$ DBR having a peak reflectivity at approximately ~300 nm. *The $B_{0.14}Al_{0.86}N$ and $Al_{0.7}Ga_{0.3}N$ layers have refractive indices of roughly 2.1[3] and 2.3[12] at 300 nm respectively. The calculated theoretical peak reflectivity closes to be 95% with a stopband of 20 nm (not shown).* Triethylboron, trimethylaluminium, trimethylgallium and $NH_3$ were used as precursors with the carrier gas being $H_2$. The detailed growth condition of the $B_{0.14}Al_{0.86}N$ layers was similar to what we previously reported.[8] The growth temperature was maintained at 910 ºC.

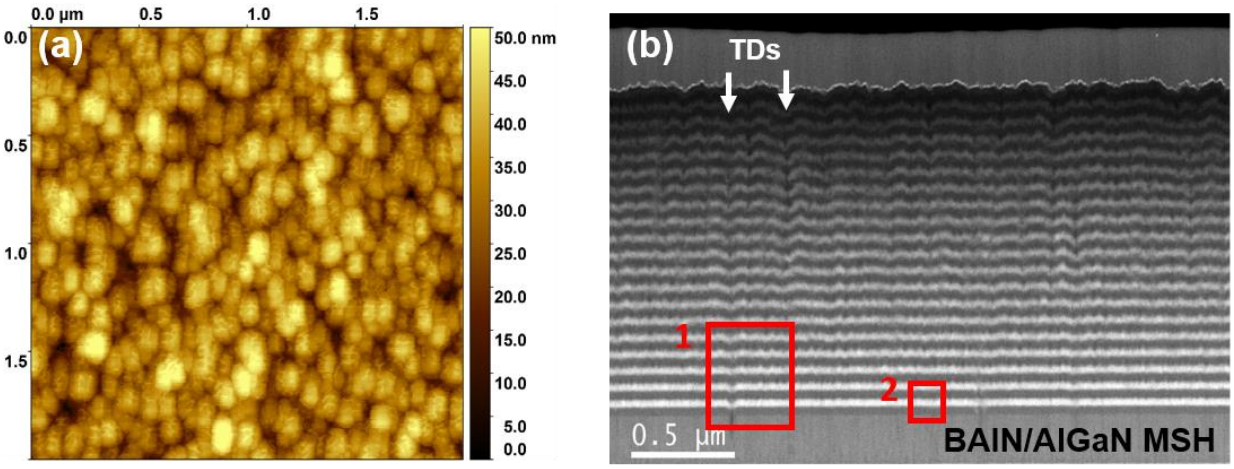


Fig. 1. (a) An AFM image and (b) a cross-sectional HAADF-STEM image of the MSH where the red boxes labeled as "1" and "2" are used in the discussion of Fig. 2 and Fig. 3, respectively.

Subsequent to the growth, we examined the surface morphology of the MSH using atomic force microscopy (AFM). As can be observed in Fig. 1 (a), the MSH surface was dominated by columnar structures with horizontal diameters between 100 and 200 nm. The RMS roughness was 6.9 nm. The formation of the columnar structures was likely caused by the BAlN layers, as the previous studies have shown that the BAlN layers possessed similar surface morphology. However, its formation mechanism was not well understood.[7,8] To understand it, high-angle annular dark-field (HAADF) scanning transmission electron microscopy (STEM) experiments were performed using an FEI probe-corrected Titan microscope operated at an acceleration voltage of 300 kV. The high-resolution transmission electron microscopy (HR-TEM) specimens were prepared by employing an FEI Helios dual-beam focused ion beam scanning electron microscope (DBFIB-SEM) system with a Ga ion source.

In Fig. 1(b) displays a cross-sectional HAADF-STEM image of the MSH. Bright and dark layers correspond to the AlGaN and BAlN layers, respectively. All the 20 pairs were present. It is noted that the MSH interface was relatively smooth for the first few pairs and became rougher along the growth direction. Eventually, this led to the columnar surface morphology that is shown in Fig. 1(a). Amid the gradual roughening was the increasing density of threading dislocations (TDs) and associated V-shape pits (V-pits) along the *c*-axis

at the MSH interface as shown in Fig. 1(b). Most of the TDs were generated within the MSH and few originated from the AlN template. On average, the distance between two V-pit centers on the MSH surface was in the range of 100 to 200 nm that was consistent with the diameter of the columnar structures from Fig. 1(a). This indicates that the columnar growth mode was caused by the V-pit formation associated with the TD.

To investigate the V-pit formation, higher magnification HAADF-STEM experiments were conducted in an area enclosed by the red box (area "1") in Fig. 1(b), including a V-pit as well as part of the AlN template and the MSH. A threading-dislocation (TD) originated from the AlN template and propagated upwards along the *c*-axis, as shown in Fig. 2(a). When the TD reached the first BAlN/AlGaN interface, a V-pit was formed, as highlighted by the red V-mark in Fig 2(a). The growth of BAlN/AlGaN interfaces followed, creating a string of the V-pits extending to the surface, as schematically shown in Fig. 2(b).

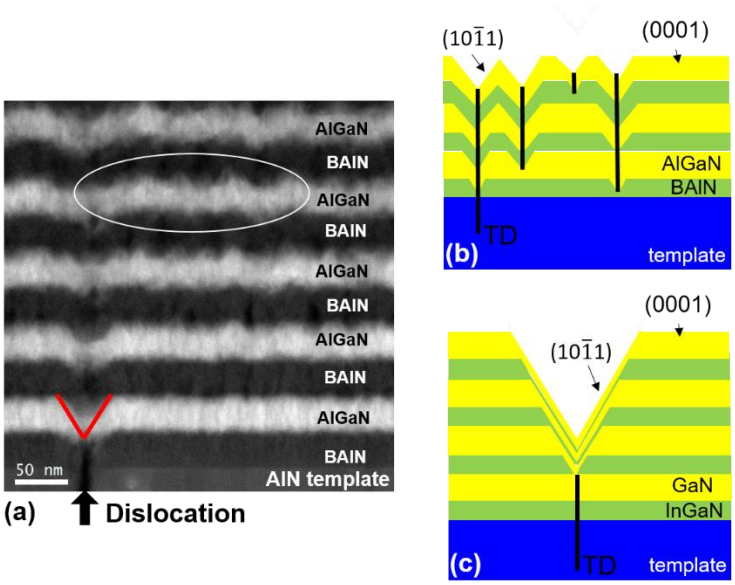


Fig. 2. (a) The HAADF-STEM image of the red box "1" in Fig. 1(b). (b) The schematic model of the V-pit formation in (b) the MSH and (c) in an InGaN/GaN heterostructure.

For the InGaN/GaN heterostructures, it has been reported that the $(10\bar{1}1)$ facet constituted the TD-induced V-pit, which was attributed to the relaxation of the stored strain around the dislocation core.[13-16] It is noted that individual V-pits in the InGaN/GaN heterostructures can keep enlarging with the growth and eventually form large inverted-pyramid surface pits, as shown in Fig. 2(c). The V-pits in our studies may also be created by the strain relaxation near the dislocation core because of the large lattice mismatch between the BAlN and AlGaN layers. However, it is important to note that the size evolution was apparently different. Although the V-pits slowly became larger along the *c*-axis, their sizes were still comparable to each other as shown in Fig. 1(b).

The respective surface kinetics can explain the difference of the V-pit size evolution between the InGaN/GaN heterostructures and the BAlN/AlGaN MSH. For the InGaN/GaN heterostructures, as the $(10\bar{1}1)$ plane is energetically less favorable for the arriving In and Ga adatoms than the (0001) plane, these adatoms with large diffusion length tend to migrate to the (0001) plane, leading to higher growth rate on the (0001) plane but reducing the growth rate on the $(10\bar{1}1)$ plane.[15,16] There have been few reports regarding the surface energy of B and Al adatoms on the (0001) and $(10\bar{1}1)$ planes. Regardless, any difference of the surface energy could be overcome by their smaller diffusion length which means that the B and Al adatoms would tend to stay on the $(10\bar{1}1)$ and (0001) planes, thereby mitigating higher growth rate on the (0001) plane and thus preventing the V-pit from rapidly growing in size. In the meantime, the Ga adatoms as a minor part of the precursors help increase the growth rate on the (0001) plane slightly, which led to slowly enlarging size for the V-pit, as shown in Fig. 1(b) and Fig. 2(b). This indicates possibly larger Ga composition of the AlGaN layer on the (0001) plane than on the $(10\bar{1}1)$ plane, which is worth future study.

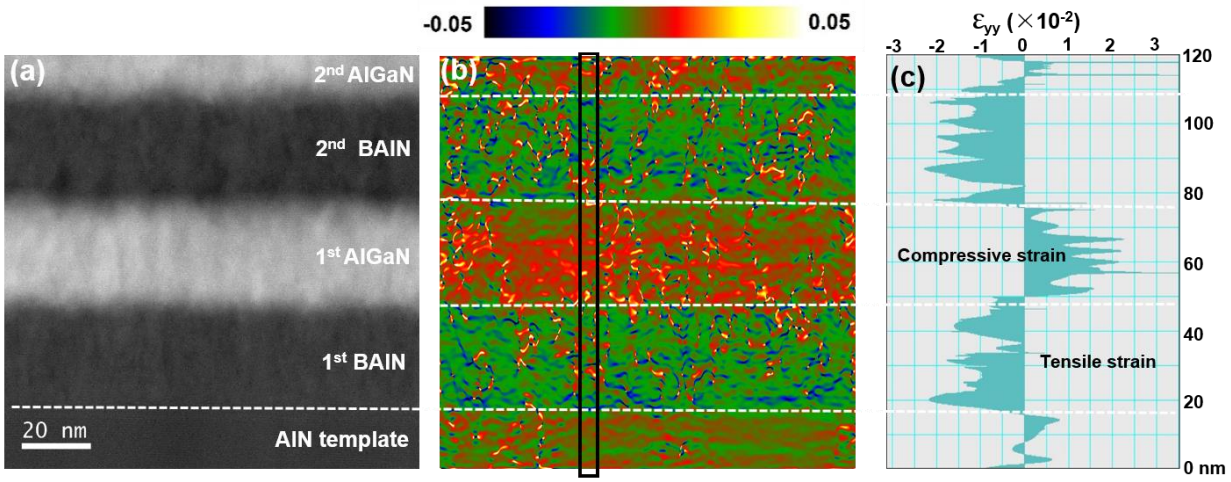


Fig. 3. A HAADF-STEM image and strain mapping of the MSH. The figures include the first four layers of the MSH and ~20 nm AlN template layer. (a) An image from the area of the red box "2" in Fig. 1 (b). (b) The corresponding strain maps obtained using the GPA for the image in (a) along the growth direction (0002), $\varepsilon_{yy}$. (c) The strain profile from the black boxed regions in (b).

As most of the V-pits were associated with the TDs generated within the MSH, it was important to understand the mechanism of the TD generation. The geometric phase analysis (GPA) was conducted on the HAADF STEM image of the MSH shown in Fig. 3(a) to analyze the strain, as the lattice mismatch between the MSH layers was considerable which might have led to dislocations due to localized strain relaxation.[1,17] The reciprocal lattice vectors, $\boldsymbol{g}$ = 0002 and $\boldsymbol{g} = 11\bar{2}0$, were selected from the image power spectrum to calculate the phase images and generate the subsequent two-dimensional (2D) strain tensors during the GPA processing.[18] The strain was referenced from the AlN template and was thus relative. Fig. 3(b) displays the map of the strain along the *c*-axis ($\varepsilon_{yy}$). The one-dimensional (1D) strain profile in the black rectangular box in Fig. 3(b) is shown in Fig. 3(c). It shows approximately −1.5% and +1% strain within the BAlN and AlGaN layers along the c-axis, respectively. This means that the BAlN and AlGaN layers were under tensile and compressive strain respectively. *These measured values slightly deviate from the theoretical strain values of the BAlN and AlGaN layers which are calculated to be -2.15% and +0.74% respectively, estimated from the lattice constants by assuming the BAlN[1,19] and AlGaN layers are fully strained to the fully-relaxed AlN template. However, this*

*deviation is reasonable because in the real case, the bottom AlN may not be fully relaxed and also we have strain relaxation via dislocation formation in the epilayers.*

In Fig. 3(b), the strain map shows that the first BAlN layer exhibited a large density of blue and yellowish spots with significantly larger strain than the layer average. They represented strain discontinuity associated with the presence of dislocations. [20,21] In the first BAlN layer, some dislocations were connected with the ones in the AlN template indicating that they were a result of the dislocation propagation from the template, while several were generated at the BAlN/AlN interface. We also noticed that the majority of the dislocations were formed within the layer. Subsequently, as the first AlGaN layer was grown, some dislocations propagated upwards to constitute most of the dislocations therein. Furthermore, some of the dislocations in the first AlGaN layer propagated into the second BAlN layer. Adding the dislocations formed therein, the dislocation density of the second BAlN layer was larger than that of the first BAlN layer *by counting the density of dislocation cores (blue and yellowish spots) from the strain map in Fig. 3(b).* We conjecture that the dislocation density continued to rise within the subsequently grown BAlN layers, which explained the observation in Fig. 1(b). This observation was different from what is normally seen in AlGaN/AlGaN heterostructures, where the dislocation density may reduce along the growth direction due to interface screening.[22] Moreover, the difference in the dislocation source between the AlGaN and BAlN layers indicates that the intrinsic growth challenges, such as short diffusion length and strong parasitic reactions,[6,8] were mainly responsible for the higher dislocation density in the BAlN layers. Because both layers were under similar strain, which, if related, generally led to misfit dislocations at the interfaces.

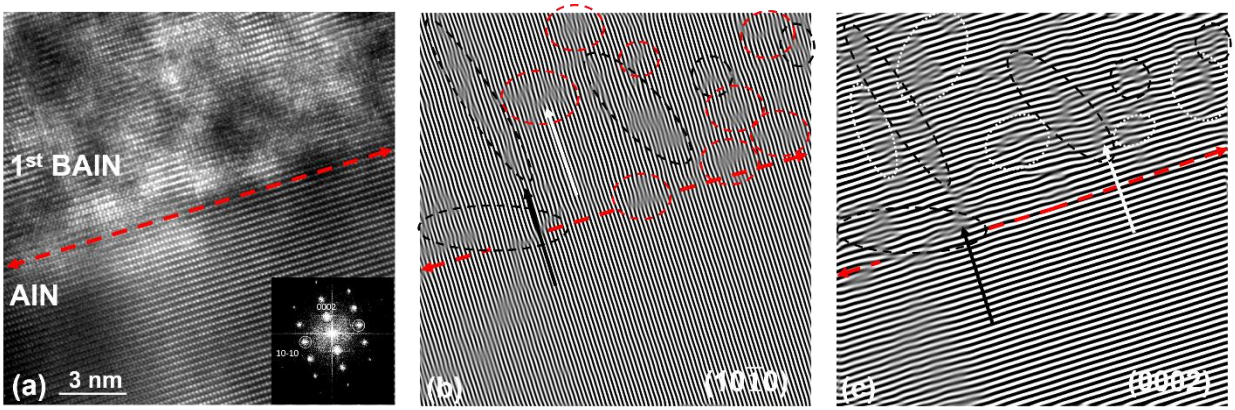


Fig. 4. (a) A [1 $\bar{1}$ 00] zone-axis HR-TEM image at the BAlN/AlN interface. The inset shows the corresponding FFT pattern. (b) and (c) are the inverse Fourier-filtered images obtained using the circled spots indicated in the inset of (a) corresponding to the (10$\bar{1}$0) and (0002) planes, respectively. Red, white

and black dashed circles represent edge, screw and mixed dislocations. White and black arrows indicate different behaviors of dislocations.

The types of dislocations were further studied by the HR-TEM focusing on the first BAlN layer. The first BAlN layer possessed significantly higher dislocation density than the AlN template, as shown in Fig. 4(a), The inverse Fourier-filtered images were obtained corresponding to the $(10\bar{1}0)$ and (0002) diffraction spots, as shown in Fig. 4(b) and (c), respectively. Based on the Burgers vectors of the dislocations in wurtzite III-nitrides,[23] the edge, screw, and mixed dislocations could be identified and were highlighted by circles of red, white, and black colors, respectively. Planar defects were not present. We found that most of the dislocations were edge and mixed dislocations, mainly at the interface. Furthermore, the dislocations either formed a continuous path along the growth direction (black arrow) or annihilated by forming loops (white arrow), which is consistent with the observation of Fig. 3(b).

In addition to the generation of various types of dislocations, we also observed twin formation within the BAlN layers. Fig. 5 exhibits a cross-sectional TEM image recorded at the 1st AlGaN/2nd BAlN/ 2nd AlGaN interface. The FFT diffraction patterns from the region enclosed by white boxes (the AlGaN layer) show a typical wurtzite structure with the same orientation, as shown in Fig. 5(b) and 5(c). However, the FFT patterns from the BAlN layer contained different orientations. Fig. 5(d) shows the same orientation as the AlGaN layer while in Fig. 5(e), we observed extra spots in the diffraction patterns that result from a mirror reflection about certain lattice planes. It contains two twin boundaries tilted by ~60°, one clockwise and the other counter-clockwise (marked as green and yellow lines) with respect to the basal plane (red line), indicating the formation of the twin structures. Their mirror planes were most likely the $\{1\bar{1}01\}$ and $\{1\bar{1}03\}$ as we recently reported.[9]

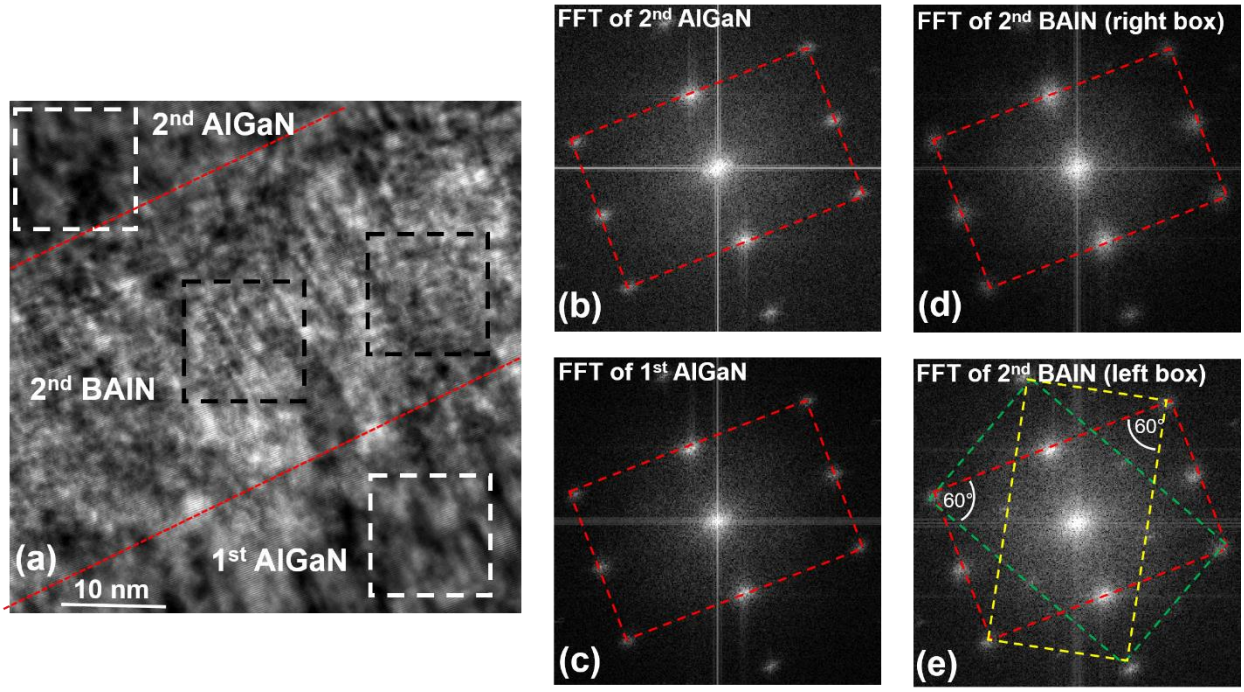


Fig. 5. (a) A [$1\bar{1}00$] zone axis HR-TEM image recorded at the 1st AlGaN/2nd BAlN/2nd AlGaN region. The red dash lines indicate the interface between the layers. Images in (b) and (c) represent the FFT patterns of the regions in the white dashed boxes marked in the 2nd AlGaN and 1st AlGaN layer in (a). Images in (d) and (e) depicted the FFT patterns of the regions in the black dashed boxes marked in the second BAlN layer in (a).

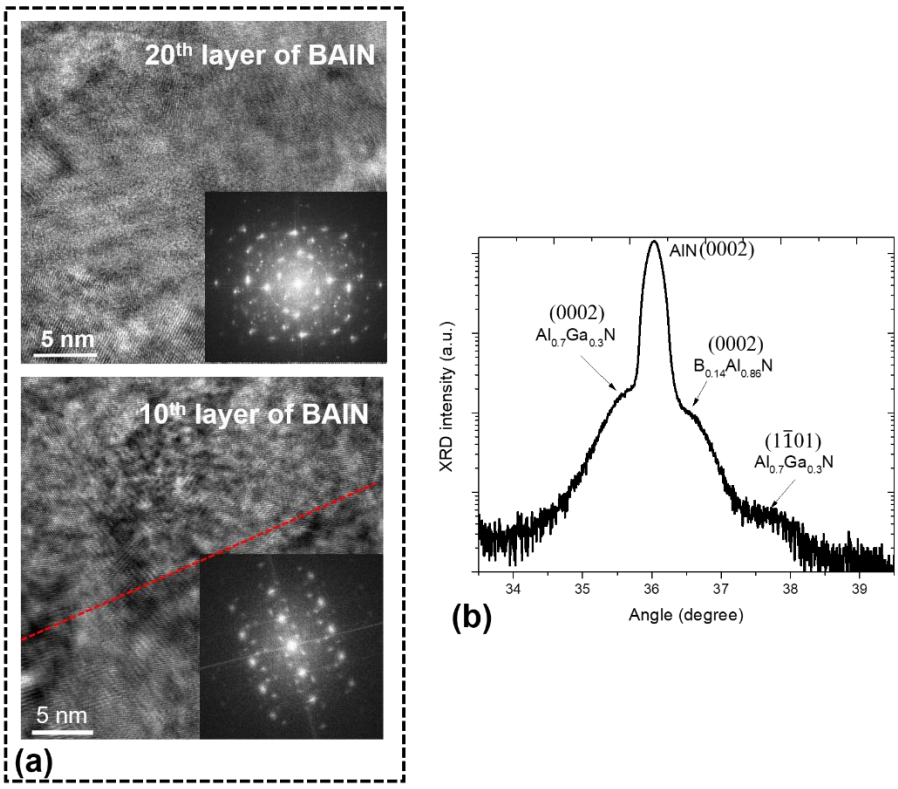


Fig. 6. (a) the HR-TEM image of the 10$^{th}$ layer and last BAlN layer in the MSH near the surface with the inset showing the corresponding FFT patterns and (b) the 2θ/ω XRD spectrum of the MSH.

Furthermore, TEM images of the 10$^{th}$ and the last layer (20$^{th}$) of BAlN were also shown. We observed that the region near the surface exhibited polycrystallinity, as shown in the inset of Fig. 6(a). However, based on the FFT of the 10$^{th}$ layer of the BAlN in the MSH, we conclude that the crystallinity was well-maintained relatively well along the (0002) except the observation of the additional dots in the FFT, indicating the formation of mis-oriented domains in the film. The X-ray diffraction (XRD) experiment confirmed the observation. In the 2θ/ω scan of the MSH shown in Fig. 6(b), the strongest peak related to AlN (0002) was located at 36.02° which also included a left and right shoulders, representing the AlGaN and BAlN (0002) peaks respectively. A weak peak at 37.72° corresponded to the wurtzite AlGaN (1$\bar{1}$01) plane, which was caused by the existence of faceted (1$\bar{1}$01) AlGaN grains in the (0002) AlGaN matrix, indicating the polycrystallization[5,7] In addition, Fig. 6(b) show no superlattice satellite peaks due to

the MSH interfacial roughness. Because of the twin structure, V-pits, and large generation of dislocations in the BAlN layers, it was difficult to understand how the wurtzite mono-crystallinity transformed into poly-crystallinity, which would be worth further studies.

In summary, this work revealed the microstructure of the $B_{0.14}Al_{0.86}N/Al_{0.70}Ga_{0.30}N$ MSH grown by MOCVD. Within the BAlN layers, a high density of the edge and mixed dislocations was formed due to the epitaxial challenges such as small B diffusion length and parasitic reactions. Some of the dislocations within the BAlN layers propagated upwards, leading to an increasing dislocation density along the *c*-axis and thus columnar surface. The V-pits were formed at the MSH interface along the threading dislocations which led to the columnar surface. The V-pit size was relatively stable because of the similar growth rates on the (0001) and $(10\bar{1}1)$ planes, which was different from the V-pits in the InGaN/GaN heterostructures. Twin structures were also observed in the BAlN layers. The MSH structure became polycrystalline near the surface, which is worth further studies. The results indicate that further optimization of the BAlN growth condition is needed for achieving high-quality BAlN/AlGaN MSH for optical and power electronics.

The KAUST authors would like to acknowledge the support of GCC Research Program REP/1/3189-01-01, Baseline BAS/1/1664-01-01, and Equipment BAS/1/1664-01-07. *The work at QU was supported by GCC Research Program GCC-2017-007.* The work at the Georgia Institute of Technology was supported in part by DARPA under Grant No. W911NF-15-1-0026 and NSF under Grant No. DMR-1410874. R.D.D. acknowledges the additional support of the Steve W. Chaddick Endowed Chair in Electro-Optics and Georgia Research Alliance.

## References

[1] Zhang M. and Li, X. 2017 Phys. Status Solidi B, **254,** 1600749

[2] Li, X., Xie, H., Ryou, J. H., Ponce, F. A., Detchprohm, T. and Dupuis, R. D. 2015 Appl. Phys. Lett. **107**, 241109

[3] Abid, M., Moudakir, T., Orsal, G., Gautier, S., Naciri, A. E., Djebbour, Z., Ryou, J.-H., Patriarche, G., Largeau, L., Kim, H. J., Lochner, Z., Pantzas, K., Alamarguy, D., Jomard, F., Dupuis, R. D., Salvestrini, J.-P., PVoss, . L. and Ougazzaden, A. 2012 Appl. Phys. Lett. **100**, 051101

[4] Sun, H., Park, Y., Li, K.-H., Torres-Castanedo, C. G., Alowayed, A., Detchprohm, T., Dupuis, R. D. and Li, X. 2017 Appl. Phys. Lett. **111,** 122106

[5] Akasaka T. and Makimoto, T. 2006 Appl. Phys. Lett. **88**, 041902

[6] Li, X., Sundaram, S., Gmili, Y. E., Moudakir, T., Genty, F., Bouchoule, S., Patriarche, G., Dupuis, R. D., Voss, P. L., Salvestrini J. P. and Ougazzaden, A. 2015 Phys. Status Solidi A **212**, 4

[7] Li, X., Sundaram, S., Gmili, Y. E., Genty, F., Bouchoule, S., Patriarche, G., Disseix, P., Réveret, F., Leymarie, J., Salvestrini J. P., Dupuis, R. D., Voss, P. L. and Ougazzaden, A. 2015 J. Cryst. Growth **44**, 119

[8] Li, X., Wang, S., Liu, H., Ponce, F. A., Detchprohm, T. and Dupuis, R. D. 2017 Phys. Status Solidi B, **254**, 1600749

[9] Wang, S., Li, X., Fischer, A. M., Detchprohm, T., Dupuis, R. D. and Ponce, F. A. 2017 J. Cryst. Growth **475,** 334

[10] Sun, H., Wu, F., Al tahtamouni, T. M., Alfaraj, N., Li, K.-H., Detchprohm, T., Dupuis, R. D. and Li, X. 2017 J. Phys. D: Appl. Phys. **50,** 395101

[11] Sun, H., Wu, F., Park, Y. J., Al tahtamouni, T. M., Li, K.-H., Alfaraj, N., Detchprohm, T., Dupuis, R. D. and Li, X. 2017 Appl. Phys. Lett. **110**, 192106

[12] Brunner, D., Angerer, H., Bustarret, E., Freudenberg, R., Höpler, R., Dimitrov, R., Ambacher, O. and Stutzmann, M. 1997 J. Appl. Phys. **82,** 5090

[13] Wu, X. H., Kapolnek, D., Tarsa, E. J., Heying, B., Keller, S., Keller, B. P., Mishra, U. K., DenBaars, S. P. and Speck, J. S. 1996 Appl. Phys. Lett. **68**, 1371

[14] Shiojiri, M., Chuo, C. C., Hsu, J. T., Yang, J. R. and Saijo, H. 2006 J. Appl. Phys. **99,** 073505

[15] Northrup J. E. and Neugebauer, J. 1999 Phys. Rev. B **60**, R8473

[16] Northrup J. E. and Neugebauer, J. 1999 Appl. Phys. Lett. **74**, 2319

[17] Dridi, Z., Bouhafs, B. and Ruterana, P. 2003 Semicond. Sci. Technol. **18**, 9

[18] Rouvière, J. L., Prestat, E., Bayle-Guillemaud, P., Hertog, M. D., Bougerol, C., Cooper D. and Zuo, J. 2013 J. Phys. Conf. Ser. **471,** 012001

[19] Liu, K., Sun, H., AlQatari, F., Guo, W., Liu, X., Li, J., Torres-Castanedo, C. G. and Li X. 2017 Appl. Phys. Lett. (in press)

[20] Rhode, S. L., Horton, M. K., Sahonta, S.-L., Kappers, M. J., Haigh, S. J., Pennycook, T. J., McAleese, C., Humphreys, C. J., Dusane R. O. and Moram, M. A. 2016 J. Appl. Phys. **119,** 105301

[21] Hÿtch, M. J., Putaux, J. and Pénisson, J. 2003 Nature **423,** 270

[22] Wang, H., Zhang, J. P., Chen, C. Q., Fareed, Q., Yang, J. W. and Khan, A. 2002 Appl. Phys. Lett. **81,** 604 (2002).

[23] Wu, X. H., Brown, L. M., Kapolnek, D., Keller, S., Keller, B., DenBaars, S. P. and Speck, J. S. 1996 J. Appl. Phys. **80**, 3228